Annals of Botany **108**: 307–319, 2011
doi:10.1093/aob/mcr161, available online at www.aob.oxfordjournals.org

ANNALS OF BOTANY
Founded 1887

An extensin-rich matrix lines the carinal canals in *Equisetum ramosissimum*, which may function as water-conducting channels

O. Leroux[1], J. P. Knox[2], B. Masschaele[3], A. Bagniewska-Zadworna[4], S. E. Marcus[2], M. Claeys[5], L. van Hoorebeke[3] and R. L. L. Viane[1,*]

[1]*Pteridology, Department of Biology, Ghent University, K. L. Ledeganckstraat 35, B-9000 Ghent, Belgium,* [2]*Centre for Plant Sciences, University of Leeds, Leeds LS2 9JT, UK,* [3]*UGCT-Department of Physics and Astronomy, Ghent University, Proeftuinstraat 86, 9000 Ghent, Belgium,* [4]*Department of General Botany, Institute of Experimental Biology, Adam Mickiewicz University, Umultowska 89, 61-614 Poznań, Poland and* [5]*Nematology, Department of Biology, Ghent University, K. L. Ledeganckstraat 35, B-9000 Ghent, Belgium*
** For correspondence. E-mail Ronnie.Viane@UGent.be*

Received: 6 January 2011 Returned for revision: 1 March 2011 Accepted: 27 April 2011 Published electronically: 12 July 2011

• *Background and Aims* The anatomy of *Equisetum* stems is characterized by the occurrence of vallecular and carinal canals. Previous studies on the carinal canals in several *Equisetum* species suggest that they convey water from one node to another.
• *Methods* Cell wall composition and ultrastructure have been studied using immunocytochemistry and electron microscopy, respectively. Serial sectioning and X-ray computed tomography were employed to examine the internode–node–internode transition of *Equisetum ramosissimum*.
• *Key Results* The distribution of the LM1 and JIM20 extensin epitopes is restricted to the lining of carinal canals. The monoclonal antibodies JIM5 and LM19 directed against homogalacturonan with a low degree of methyl esterification and the CBM3a probe recognizing crystalline cellulose also bound to this lining. The xyloglucan epitopes recognized by LM15 and CCRC-M1 were only detected in this lining after pectate lyase treatment. The carinal canals, connecting consecutive rings of nodal xylem, are formed by the disruption and dissolution of protoxylem elements during elongation of the internodes. Their inner surface appears smooth compared with that of vallecular canals.
• *Conclusions* The carinal canals in *E. ramosissimum* have a distinctive lining containing pectic homogalacturonan, cellulose, xyloglucan and extensin. These canals might function as water-conducting channels which would be especially important during the elongation of the internodes when protoxylem is disrupted and the metaxylem is not yet differentiated. How the molecularly distinct lining relates to the proposed water-conducting function of the carinal canals requires further study. Efforts to elucidate the spatial and temporal distribution of cell wall polymers in a taxonomically broad range of plants will probably provide more insight into the structural–functional relationships of individual cell wall components or of specific configurations of cell wall polymers.

Key words: Extensin, carinal canal, *Equisetum*, immunolabelling, cell wall.

INTRODUCTION

Equisetum is a genus of approx. 15–25 extant hollow-stemmed taxa (Milde, 1867; Sadebeck, 1902; Smith, 1955; Hauke, 1963, 1978, 1990; Guillon, 2007), which are the only link to a group of extinct, diverse and dominant pteridophytes (Brongniart, 1828; Frank, 1877; Eames, 1936; Hirmer, 1938; Emberger, 1944; Stewart, 1983; Bateman, 1991; Rothwell, 1996; Stanich *et al.*, 2009). In the last two decades there has been an increased interest in the phylogeny (Des Marais *et al.*, 2003; Guillon, 2004, 2007), biomechanics (Spatz *et al.*, 1998; Speck *et al.*, 1998; Spatz and Emanns, 2004) and cell wall biology (Popper and Fry, 2004; Fry *et al.*, 2008; Gierlinger *et al.*, 2008; Sørensen *et al.*, 2008; Currie and Perry, 2009) of this remarkable genus.

Recent phylogenetic studies (Kenrick and Crane, 1997; Pryer *et al.*, 2001; Qiu *et al.*, 2007; Karol *et al.*, 2010) separate Lycophyta from the core pteridophytes, and unite Equisetaceae to the true ferns [Pteridophyta *sensu stricto* (*s.s.*)] as a monophyletic group. In recent cell wall research, *Equisetum* has received a lot of attention as a mixed-linkage $(1 \rightarrow 3)$ $(1 \rightarrow 4)$-β-D-glucan (MLG), previously thought only to occur in Poales cell walls, was found abundantly in *Equisetum* cell walls (Fry *et al.*, 2008; Sørensen *et al.*, 2008). The discovery of this polysaccharide in a land plant outside Poales suggested novel cell wall architectures unlike either type I or type II cell walls (Knox, 2008).

The general morphology as well as the anatomy of the mature stem, first described in detail by Bischoff (1828), Brongniart (1828) and Milde (1865), is so characteristic that the genus has been distinguished correctly from other superficially similar plant taxa since Tournefort (1719; for a review, see Milde, 1867). A transverse section of the internode shows a pattern of sub-epidermal strengthening tissue and chlorenchyma, vallecular canals in the cortex opposite the furrows, and carinal canals opposite the ridges. The vascular bundles are always positioned

opposite a ridge, forming a ring surrounding the central cavity (Ogura, 1972). Westermaier (1884) was the first to suggest that carinal canals, which are protoxylem lacunae, are water-conducting canals. This was later accepted by Sykes (1906), Schaffner (1908), Barrat (1920) and Bierhorst (1958*a*). Brogniart (1828) and Cormack (1893) pointed out that the carinal canals are not continuous from one internode to the next, and that nodal xylem elements convey water from one canal to another. These nodal xylem elements were later studied by Sykes (1906) and Bierhorst (1958*a*, *b*).

In light of the recent discovery of mixed-linkage glucans in *Equisetum* cell walls (Fry *et al.*, 2008; Sørensen *et al.*, 2008), and the observation of complex distribution patterns of cell wall epitopes during a comparative study of fern cell walls, we decided to perform a detailed study focusing on the distribution patterns of cell wall epitopes in *Equisetum* stems. Our immunocytochemical study revealed a restricted occurrence of extensin epitopes to the carinal canal linings. Therefore, we also re-examined the ontogeny and structure of these canals, with attention given to the nodal anatomy, as this has been poorly documented in the recent literature.

MATERIALS AND METHODS

Plant material

Plant material of *Equisetum ramosissimum* was collected in Spain (La Palma, Caldera de Taburiente, Galeria Aridane, 1100 m, Viane 8118) and kept in our living collection at the Ghent Botanical Garden, Belgium.

Histology

Internodal and nodal segments of mature and young *Equisetum* stems were fixed overnight in FAA [50 % (v/v) ethanol, 5 % (v/v) acetic acid and 5 % (v/v) commercial formalin in distilled water], dehydrated in an ethanol series and embedded in Technovit 7100 (Heraeus Kulzer, Wehrheim, Germany) following Leroux *et al.* (2007*a*). Transverse sections of 4 μm were cut with a Microm HM360 microtome (Microm International GmbH, Walldorf, Germany) equipped with a holder for glass knives, dried on Vectabond-coated (Vector Laboratories, Burlinghame, CA, USA) slides, stained with an aqueous 0·05 % (w/v) solution of toluidine blue O (Merck, Darmstadt, Germany, C.I. No. 52040) in 0·1 % (w/v) $Na_2B_4O_7$ (pH 8·5) and mounted in DePeX (Gurr, BDH Laboratory, UK). Phloroglucinol/HCl staining was performed on fresh hand-cut sections using 2 % (w/v) phloroglucinol in 95 % (v/v) ethanol for 5 min, and subsequently mounting in 33 % (v/v) hydrochloric acid. For Maüle staining, fresh hand-cut sections were immersed in 1 % (w/v) potassium permanganate for 10 min at room temperature and then washed twice with 3 % hydrochloric acid. Sections were observed with a Nikon Eclipse E600 microscope and images were recorded using a Nikon digital camera DXM1200.

X-ray computed tomography and drawings

Samples fixed in FAA and processed following Leroux *et al.* (2009) were scanned at the centre for computed tomography (UGCT) of Ghent University (Masschaele *et al.*, 2007). For the measurements we used an in-house scanner, the main components of which are: an open type Hamamatsu nanofocus X-ray tube (L10711); a second sealed type Hamamatsu microfocus (L9181-02); a high resolution CCD camera with fibreoptic taper from Photonic Science; a Varian amorphous silicon flat panel detector (Paxscan 2520 with CsI scintillator); and a sample manipulator which can move the samples with 5 ° of freedom. The samples were scanned with the L9181 tube at 70 kV and 60 μA in order to obtain high contrast and high spatial resolution. The samples were rotated from 0 ° to 360 ° in steps of 0·45 °. The Varian detector was set to an exposure time of 400 ms, and six frames were averaged per rotation step to increase the statistics of the images. The samples were magnified 42 times in order to reach a voxel size of 3 μm in the CT images. The raw projection images were processed into CT slices with Octopus. Octopus is a user-friendly, system-independent, reconstruction package developed and commercialized by Ghent University (www.inct.be). After the reconstruction >800-cross sections through the sample volume were obtained. The software program VGStudio Max (http://www.volumegraphics.com) was used to create the 3-D renderings. Drawings were based on a selection of virtual cross-sections and were made with CorelDRAW Graphics Suite 12.

Transmission electron microscopy

Equisetum stems were dissected in order to produce blocks measuring approx. 2 mm length on all sides. They were fixed with 2 % (w/v) paraformaldehyde and 2 % (v/v) glutaraldehyde in a 0·1 M cacodylate buffer pH 6·9 for 24 h at 4 °C, post-fixed in 2 % (v/v) osmium tetroxide for 3 h, washed in the same buffer and dehydrated in a step gradient of ethanol. The samples were transferred to 100 % alcohol/Spurr's resin (1:1) at 4 °C overnight, brought to 100 % alcohol/Spurr's resin (1:2) for 8 h (4 °C), and transferred to 100 % Spurr's resin and left overnight at 4 °C. Polymerization was performed at 70 °C for 16 h. Sections of 70 nm thickness were made using a Reichert Ultracut S ultramicrotome (Leica, Vienna, Austria). Formvar-coated single slot copper grids were used. Sections were stained with a Leica EM stain for 30 min in uranyl acetate at 40 °C and 10 min in lead citrate stain at 20 °C. The grids were examined with a JEM-1010 electron microscope (Jeol Ltd, Tokyo, Japan) equipped with imaging plates which were scanned digitally (Ditabis, Pforzheim, Germany).

Scanning electron microscopy

Longitudinal hand-cut root sections were fixed in FAA, dehydrated in a graded ethanol series followed by a graded acetone series, and dried in a critical point dryer (Balzers CPD-030) using CO_2 as a transition fluid. Dried sections were mounted on clean aluminium stubs with double-sided adhesive graphite tabs. Mounted specimens were coated with gold (12–15 nm thick) using a Balzers SPD-050 sputter coater. Sections were photographed digitally using an EVO40 scanning electron microscope (Carl Zeiss, Germany).

Immunocytochemistry

For indirect immunofluorescence labelling, hand-cut sections of internodal segments were made. A range of highly specific cell wall-directed probes available was used to evaluate the presence of major cell wall polymers including pectins, xyloglucans, (glucogalacto)mannans, (arabino)xylans and extensins (see Table 1).

The sections were incubated in 5 % (w/v) milk protein in phosphate-buffered saline (MP/PBS) for 5 min to block non-specific binding sites. Sections were then incubated with primary rat monoclonal antibodies (JIM5, JIM7, LM19, LM20, LM5, LM6, LM13, LM16, LM10, LM11, LM15, LM21, LM1 and JIM20; for references see Table 1) diluted 1:10 in MP/PBS for at least 1 h. The sections were washed with several changes of PBS prior to incubation with the secondary antibody, anti-rat IgG linked to fluorescein isothiocyanate (FITC; Sigma) diluted 1:100 in 5 % (w/v) MP/PBS for 1 h. CCRC-M1, a monoclonal antibody developed in mice (Puhlmann *et al.*, 1994), was used in 1:5 dilutions, and binding was visualized with a 50-fold diluted mouse anti-his monoclonal antibody (Sigma) in MP/PBS for 1·5 h. The binding of CBM3a (Blake *et al.*, 2006) was assessed by a three-stage immunolabelling procedure. After incubating in MP/PBS containing 40 μg mL^{-1} CBM3a protein for 1·5 h, sections were washed in PBS at least three times and incubated with a 100-fold dilution of mouse anti-his monoclonal antibody (Sigma) in MP/PBS for 1·5 h. Following washing with PBS, anti-mouse IgG linked to FITC was applied for 1·5 h at a 50-fold dilution in MP/PBS. Labelling with the Biosupplies 400-3 anti-mixed-linkage glucan antibody was performed as described elsewhere (Meikle *et al.*, 1994). Cellulose was stained with Calcofluor White M2R fluorochrome (fluorescent brightener 28, Sigma, 0·25 μg mL^{-1} in dH_2O). Subsequently, all sections were washed in PBS buffer three times before mounting in a glycerol-based anti-fade solution (Citifluor AF1, Citifluor Ltd, UK). Recent studies showed that cell wall epitopes can be masked and, where appropriate, we performed pectate lyase treatments as described by Marcus *et al.* (2008). Immunofluorescence was observed with a microscope equipped with epifluorescence irradiation (Olympus BX-61) and images were captured with a Hamamatsu ORCA285 camera and prepared with Improvision Volocity software.

Peroxidase assay

In situ peroxidase activity was detected by treatment of fresh hand-cut sections in 5 mg mL^{-1} 3,3′-diaminobenzidine (DAB)-HCl, pH 3·8, re-buffered to pH 5·8 immediately before use. Subsequently 1 mM H_2O_2 was added and incubation was performed at room temperature for 5 min.

RESULTS

Anatomy of the internode

Cross-sections through mature internodes of *E. ramosissimum* show the typical internodal anatomy described in the Introduction (Fig. 1A), characterized by strengthening tissues in the ridges, carinal (Fig. 1A–C) and vallecular (Fig. 1A, D) canals as well as a central cavity occupying nearly half of the total diameter (Fig. 1A). The vascular bundles are enclosed by a common internal and external endodermis (Fig. 1B). In each vascular bundle, two groups of xylem elements, which will further be referred to as metaxylem, are positioned laterally at both sides of the phloem (Fig. 1B). In longitudinal sections of mature internodes, the lining of the carinal canals is smooth apart from occasional protoxylem rings (Fig. 1C), whereas in vallecular canals remnants of disrupted parenchyma cells are visible (Fig. 1D). In older internodes, the parenchyma cell walls facing the carinal canals are slightly thickened. Figure 1E shows a transverse section of a young internode surrounded by a leaf sheath, showing six developing vascular bundles, but without fully developed carinal or vallecular canals. A detail of a vascular bundle (Fig. 1F) shows both protophloem and protoxylem, as well as some very small carinal canals, which developed after disruption and/or dissolution of protoxylem elements. Vallecular canals and central cavities were seen to develop through disruption of cortex and pith parenchyma, respectively, prior to the differentiation of the metaphloem and metaxylem (data not shown). In all young internodes studied, the central cavities developed prior to the vallecular canals, and metaxylem differentiated after the elongation of the internodes had ceased (data not shown).

Immunofluorescence labelling of cell wall components and lignin staining

Several monoclonal antibodies and a carbohydrate-binding module were used to examine the presence of major cell wall constituents including pectins, cellulose, hemicelluloses and extensins in *E. ramosissimum* stems (Fig. 2). The results are summarized in Table 1 and relevant and specific binding patterns are discussed here. Figure 2A is a combined image of Calcofluor staining and red autofluorescence. Calcofluor, with a high affinity for (1 → 4)-β-D-glucans and (1 → 3)-β-D-glucans, stained all cell walls, except metaxylem secondary cell walls, Casparian strips and the lining of the carinal canals. Guard cells as well as phloem cells (Fig. 2A) were intensively stained. Red autofluorescence of Casparian strips of both the internal and external endodermis and of the metaxylem secondary cell walls was evident (Fig. 2A). The source of this autofluorescence is, however, unclear. The LM1 and JIM20 antibodies, both recognizing extensin epitopes, bound to the lining of the carinal canals (Fig. 2B). Extensin epitopes are not restricted to the lining of carinal canals, as pectate lyase treatment revealed a very weak binding of LM1 to cell wall corners of the cortex parenchyma (data not shown). The monoclonal antibodies JIM5 and LM19, which bind to homogalacturonan with a low degree of methyl esterification, clearly labelled the lining of the carinal canals as well as most parenchymatous cell walls in the stem (Fig. 2C). Binding of JIM5 was strongest at cell wall corners and to the middle lamellae, whereas it bound relatively weakly to primary cell walls. In contrast, JIM7 and LM20, recognizing homogalacturonan with a high degree of methyl esterification, bound to all primary cell walls but not to the lining of the carinal canal (Fig. 2D). LM5, binding to (1 → 4)-β-D-galactan, labelled all parenchymatous cell walls in a similar way to JIM7 (Fig. 2E). The (1 → 5)-β-L-arabinan epitope, recognized by LM6, occurred in all parenchyma cell

TABLE 1. *Tissue-specific distribution of cell wall epitopes in* Equisetum ramosissimum *internodes*

		Epidermis	Guard cells	Subsidiary cells	Strengthening tissue	Chlorenchyma	Cortex parenchyma	Lining carinal canal	Endodermis	Lining vallecular canal	Lining central cavity	Xylem	Parenchyma surrounding vascular bundle	Phloem
JIM5[1]	Partially Me-HG/ de-esterified HG	−	+	+	+†††	+†††	+†††	+	+	++	++	+^{p}	+†††	+
JIM7[1]	Partially Me-HG	−	−	−	+††	+	+	+	+	+	+	−	+	+
LM19[2]	Partially Me-HG/ de-esterified HG	−	+	+	+†††	+	+	+	+	++	++	+^{p}	+	+
LM20[2]	Partially Me-HG	−	−	−	+^{p}	+	+	+	+	+	+	−	+	+
LM5[3]	(1 → 4)-β-D-galactan	−	−	−	+††	+	+	+	+	+	+	−	+	+
LM6[4]	(1 → 5)-β-L-arabinan	−	+	+	+††	+	+	+	+	+	+	−	+	+
LM13[5]	Linearized (1 → 5)-β-L-arabinan	−	−	+	−	−	−	−	+	−	−	−	−	−
LM16[5]	Processed arabinan	−	+	−	−	−	−	−	−	−	−	−	−	−
LM10[6]	(1 → 4)-β-D-xylan	−	+	−	−	−	−	−	−	−	−	+^{s}	−	−
LM11[6]	(1 → 4)-β-D-xylan/ arabinoxylan	−	+	−	−	−	−	−	−	−	−	+^{s}	−	−
LM15[7]	XXXG motif of xyloglucan	−	+	−	− (++ ^{p})	− (+)	− (±)	− (±)	−	+	+	−	−	+
CCRC-M1[8]	α-L-Fucosylated xyloglucan	−	−	−	+^{p} (++ ^{p})	− (±)	− (±)	− (±)	−	+	+	−	−	+
Biosupplies 400-3[8]	(1 → 3) (1 → 4)-β-glucan	−	−	−	+††	−	+	−*	−	−	−	−	−	−
LM21[10]	(galacto) (gluco)mannan	+	−	+	+	+	+	−	+	+	+	+^{s}	+	−
LM22[10]	(gluco)mannan	+	−	+	−	−	−	−	−	−	−	−	−	−
CBM27[10]	Mannan	+	−	+	+	+	+	−	+	+	+	+^{s}	+	−
CBM3a[11]	Crystalline cellulose	+	+	+	+	+	+	++	+	++	++	+	+	+
Biosupplies 400-2[12]	(1 → 3)-β-glucan	−	−	−	−	−	−	−	−	−	−	−	+†	−
LM1[13]	Extensin	−	− (±)	−	−	−	− (±)	+	−	−	−	−	−	−
JIM20[14]	Extensin	−	±	−	−	−	−	+	−	−	−	−	−	−

++ strong binding; + binding; ± weak binding; † binding to protophloem cell walls and oblique transverse cell walls of the metaphloem; †† binding restricted to the inner cell wall region; ††† binding to middle lamellae and cell wall corners; ^{p} binding restricted to the primary cell wall; ^{s} binding restricted to the secondary cell wall; *binding to cortical parenchyma located between the vallecular canals and the chlorenchyma. Additional binding patterns revealed after pectate lyase treatment are indicated in parentheses.

References for binding specificity: [1]Clausen *et al.* (2003); [2]Verhertbruggen *et al.* (2009*b*); [3]Jones *et al.* (1997); [4]Willats *et al.* (1998); [5]Verhertbruggen *et al.* (2009*a*); [6]McCartney *et al.* (2005); [7]Marcus *et al.* (2008); [8]Meikle *et al.* (1994); [9]Puhlmann *et al.* (1994); [10]Marcus *et al.* (2010); [11]Blake *et al.* (2006); [12]Meikle *et al.* (1991); [13]Smallwood *et al.* (1995); [14]Smallwood *et al.* (1994).

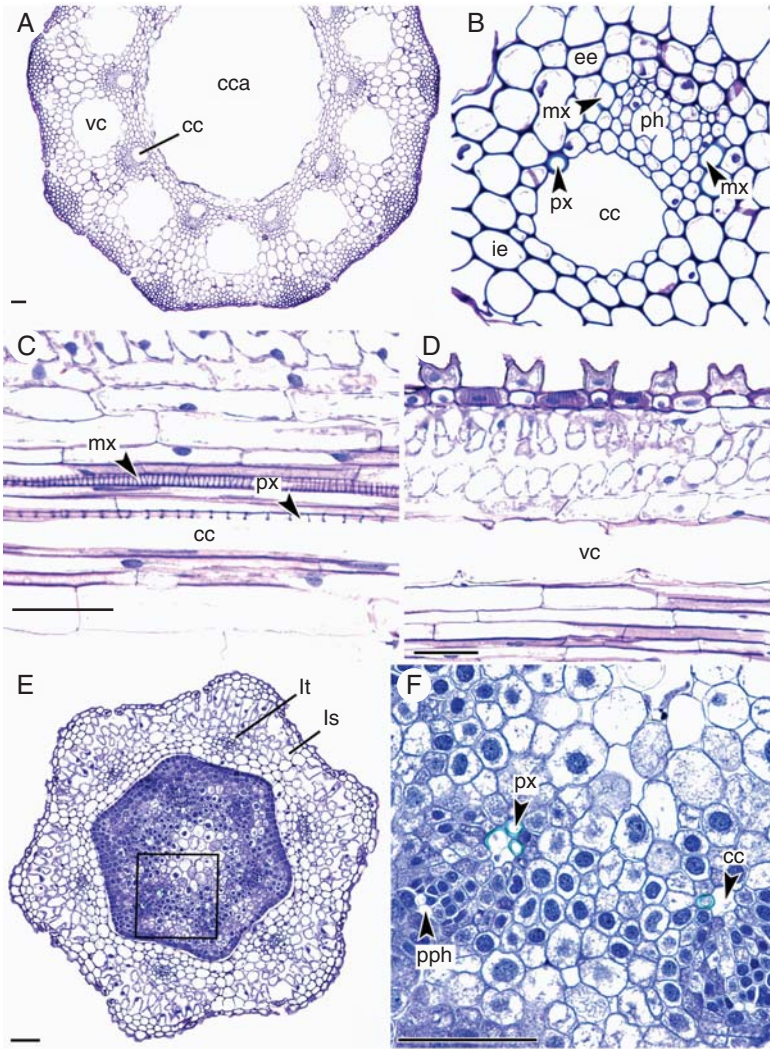

FIG. 1. Transverse (A, B, E, F) and longitudinal (C, D) sections through mature (A–D) and young (E, F) internodes of *Equisetum ramosissimum*. (A) An internode showing the central cavity (cca), carinal (cc) and vallecular (vc) canals. (B) A vascular bundle consisting of a carinal canal (cc) with protoxylem (px) elements, metaphloem (ph) and metaxylem elements (mx). A ring of vascular bundles enclosed by an internal (ie) and external (ee) endodermis. (C) Part of a vascular bundle showing the carinal canal (cc) with a smooth surface, protoxylem (px) with annular thickenings, and a scalariform metaxylem (mx). (D) Epidermis with silicifying papillae and cortex with vallecular canals (vc) with a rough surface caused by disintegrated cells. (E) A young internode surrounded by a leaf sheath (ls) with leaf traces (lt). Protoxylem starting to disintegrate and forming small carinal canals. (F) Detail (indicated in E) of differentiating vascular bundle with protophloem (pph) and protoxylem (px). Metaxylem and metaphloem are as yet undifferentiated. Scale bars = 100 μm.

walls as well as in subsidiary and guard cell walls. Two other anti-arabinan antibodies, LM13 and LM16, bound, respectively, to the cell walls of subsidiary and guard cells of the stomatal complex of *E. ramosissimum*, confirming the results shown by Verhertbruggen *et al.* (2009*a*). CBM3a, a carbohydrate-binding module which recognizes crystalline cellulose, bound to all cell walls, including the lining of the carinal canals (Fig. 2F). Binding of the anti-xylan antibodies LM10 and LM11 was restricted to the secondary cell walls of the scalariform metaxylem tracheids (Fig. 2G) and to the guard cell walls. Mannan epitopes, recognized by LM21, were especially abundant in all parenchymatous cell walls enclosed by the inner and outer endodermis (Fig. 2H), and those of the epidermis and strengthening tissue. Pre-treatment with pectate lyase showed the presence of the LM21 epitope in all cell walls, including those of the phloem. An anti-mixed-linkage glucan antibody only bound to the inner wall regions of the cells of the strengthening tissue (Fig. 2I) and to the walls of some cortical parenchyma cells located between the chlorenchyma and the vallecular canals. It is of interest that LM15, an antibody binding to the XXXG motif of xyloglucan, strongly bound to sieve cells of the phloem (Fig. 2J) and to guard cells, but weakly to the lining of vallecular canals and the central cavity. However, LM15 reacted weakly with the lining of the carinal canals after pectate lyase treatment (Fig. 2K). CCRC-M1, which recognizes fucosylated xyloglucan, bound to the phloem cell walls and strengthening tissue, and to the lining of vallecular and central canals. Pectate lyase treatment unmasked this epitope in the lining of carinal canals (Fig. 2L).

In order to assess the presence of lignins, fresh hand-cut sections were stained with Wiesner (Fig. 3A–D) and Maüle reagent. These stains both gave the same result, showing the

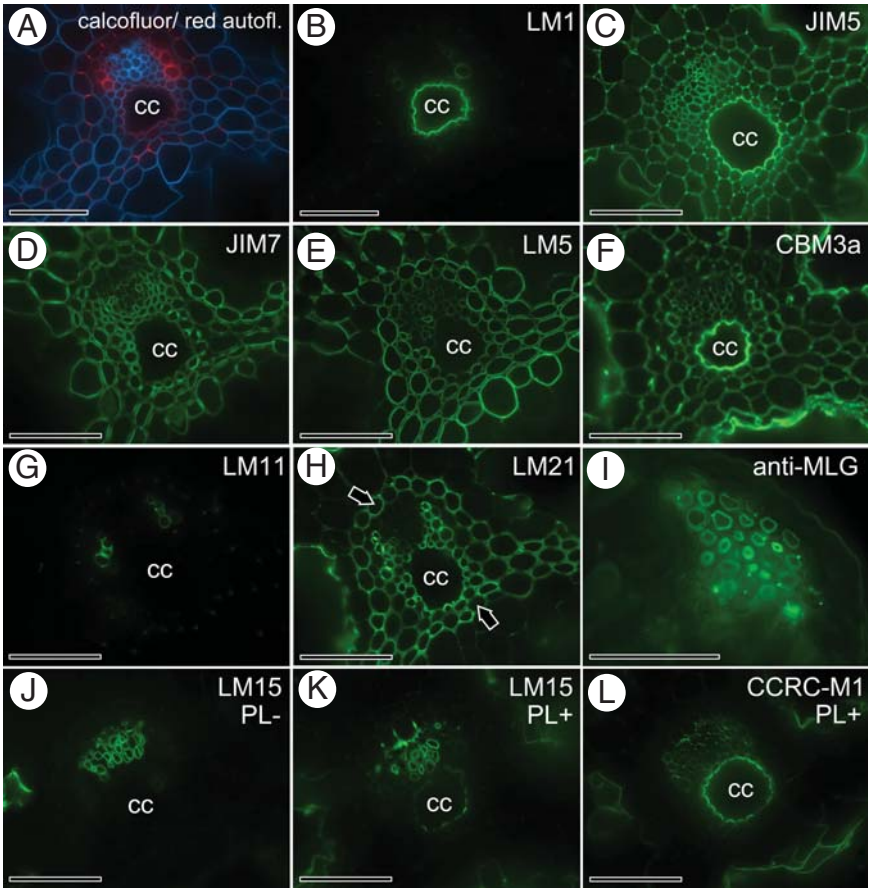

FIG. 2. Immunolabelling of transverse sections through *E. ramosissimum* internodes using monoclonal antibodies and a carbohydrate-binding module directed against different cell wall epitopes. (A) Combined image of calcofluor staining (blue), and red autofluorescence of Casparian strips. (B) LM1 epitope (extensin) restricted to the lining of carinal canals; the same section as in (A). (C) Binding of JIM5 (pectic homogalacturonan with high levels of esterification) to the lining of carinal canals and middle lamellae of parenchymatous cells. (D) JIM7 epitope (pectic homogalacturonan with low levels of esterification) occurring in primary cell walls but absent from carinal canal lining. (E) Binding pattern of LM5 (anti-galactan) similar to that of JIM7. (F) CBM3a binding to all cell walls as well as to the lining of carinal canals. (G) LM11 (anti-xylan) binding to metaxylem elements. (H) LM21 mannan epitopes detected in walls of the endodermis (arrows) and enclosed pericycle and parenchyma, and in the the lining of vallecular canals. (I) Anti-MLG antibody binding to inner cell wall regions of strengthening tissue. (J) LM15 (anti-xyloglucan) strongly binding to phloem cell walls, but weakly to lining of vallecular canals. (K, L) Effect of pectate lyase treatment showing LM15 (K) and CCRC-M1 (L) binding to the lining of carinal canals. cc, carinal canals. Scale bars = 100 μm.

presence of lignin in the xylem tracheids and Casparian strips, and its absence in the cell walls of the strengthening tissue (Fig 3A, C). A peroxidase activity assay was performed and, in the presence of exogenous hydrogen peroxidase, DAB strongly stained the cell walls of the endodermis, epidermis, the cortical parenchyma, the metaxylem and the lining of the carinal canals (Fig. 3E). The cell walls of the remaining tissues, including the phloem, pericycle and the parenchyma enclosed by the endodermis, and, surrounding the vallecular canals and the central cavity, were not stained (Fig. 3E).

Electron microscopy

Transmission electron microscopy showed the absence of intercellular spaces in the tissues enclosed by the internal and external endodermis. Instead, these spaces (Fig. 4A) are filled with intensely stained materials, comparable with the middle lamellae. A similar material also lines the carinal canals (Fig. 4A, B). A detail of the border of a vallecular canal shows cell wall remnants of disrupted parenchyma cells (Fig. 4C); an electron-dense coating similar to that present in the carinal canals was not found. The surface of the carinal and vallecular canals, as well as that of the central cavities was also studied using scanning electron microscopy. Carinal canals have a smooth surface (Fig. 4D), occasionally with attached protoxylem rings (not shown). In contrast, both the central cavity (Fig. 4E) and the vallecular canal (Fig. 4F) are characterized by a rough surface. Xylem elements in the nodes are short and show multiseriate pitting (Fig. 4G), whereas the internodal metaxylem elements have a scalariform thickening (Fig. 4H).

Nodal interconnection of carinal canals

In the node, leaf and branch traces depart and the position of vascular bundles of successive internodes changes. Nodes show a different arrangement of xylem and phloem elements compared with the internode (Figs 1A and 5C), and have an ectophloic siphonostele (Fig. 5C) with leaf gaps as well as branch gaps. Longitudinal median sections (Fig. 5A) show

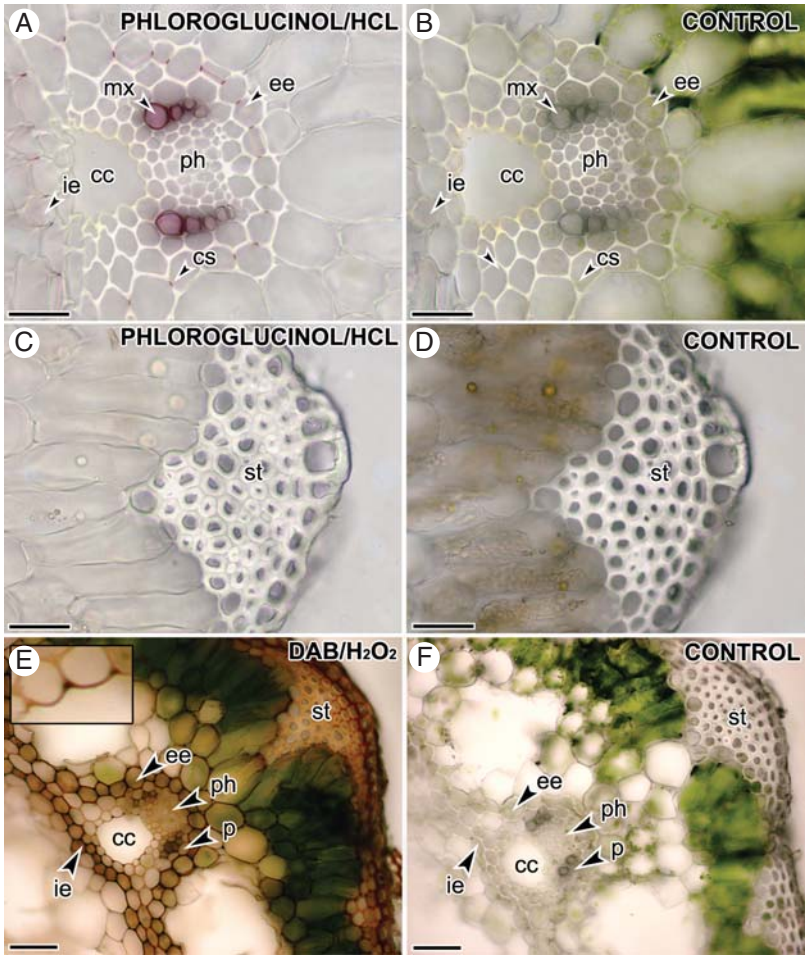

FIG. 3. Localization of lignins through phloroglucinol/HCl staining (A–D) and determination of peroxidase activity using DAB/hydrogen peroxide (E–F) in transverse sections of *E. ramosissimum* stems. (A, B) Walls of the metaxylem tracheids and Casparian strips of internal (ie) and external endodermis (ee) stain intensely red, suggesting the presence of lignins. (C, D) Walls of the strengthening tissue are uncoloured, suggesting the absence of lignins. (E, F) Walls of the epidermis, cortical parenchyma, internal (ie) and external endodermis (ee), and lining of the carinal canal (inset) stain blackish-brown, whereas phloem (ph), pericycle (p), strengthening tissue (st), parenchyma enclosed by double endodermis, and parenchyma surrounding vallecular canals and the central cavity remain unstained. Scale bars = 100 μm.

the diaphragm which forms an interruption between the central cavities of consecutive internodes. Furthermore, the vallecular canals are completely interrupted in the node (Fig. 5C, F), while the carinal canals are connected to the nodal xylem (Fig. 5A, B).

Good-quality serial sectioning – without the loss of several sections – of *Equisetum* nodes was difficult due to the high silica content of the cell walls. The internode–node–internode transition in *E. ramosissimum* was therefore also studied by X-ray CT (see Supplementary Data Fig. S1 and video). In addition, this method allowed the generation of perfectly aligned serial virtual sections in both transverse and longitudinal planes. The schematic drawings in Fig. 6 were largely based on these aligned virtual sections. In each vascular bundle the nodal transition starts with the gradual increase of xylem elements towards the carinal canals (Fig. 6B). Closer to the node, the carinal canals are gradually replaced by xylem elements (Fig. 6C), which bulge out and first form branch traces later followed by leaf traces (Fig. 6C, D). In contrast to other *Equisetum* species, where branches are formed between all leaf traces (Bischoff, 1828, 1834; Stenzel, 1861; Gwynne-Vaughan, 1901; Browne, 1912), branches develop irregularly in *E. ramosissimum*. Leaf traces are formed opposite each ridge and in the prolongation of the original vascular bundle (Fig. 6D). The departing leaf traces are clearly associated with narrow leaf gaps as shown in Fig. 5D. After closing of the leaf gaps, a short ectophloic siphonostele, often still interrupted by branch gaps, is formed in the node (Figs 5C and 6E). At this level, the central cavity is replaced by a diaphragm and the vallecular canals are strongly reduced in diameter. As we pass upward above the departure of the leaf traces, the nodal xylem diminishes and becomes separated (Fig. 6F, G), with each meristele surrounded by an individual endodermis (Fig. 5E). The typical internodal arrangement of vascular bundles with carinal canals and lateral xylem soon reappears (Fig. 6H), as well as the internal and external endodermis. Vallecular canals as well as the central cavity reappear, and the leaf sheath is separated (Fig. 6H, I). Each internode–node–internode transition shows an alternation in the position of the vascular bundles. The midribs of the leaves, which are

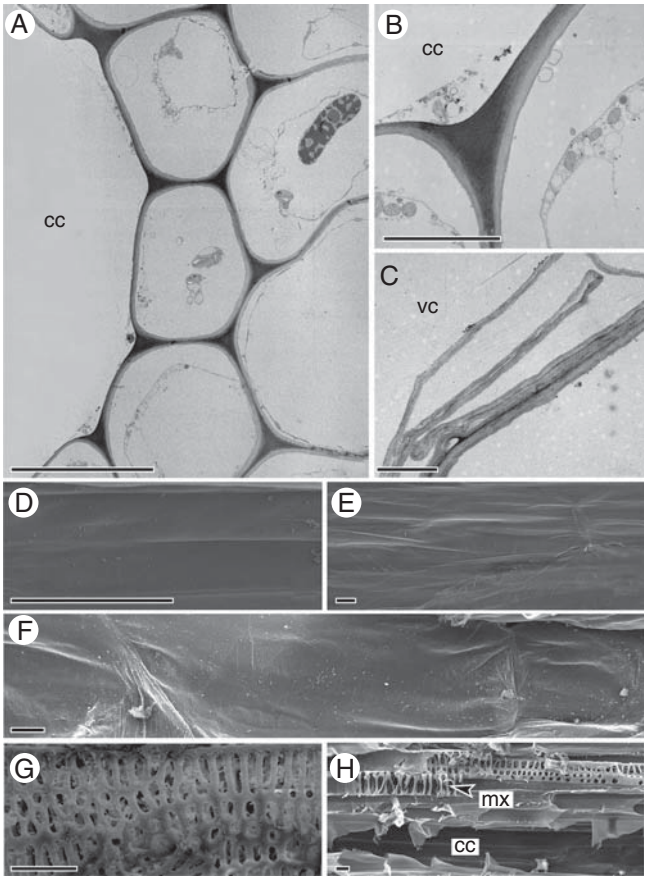

FIG. 4. Transmission (A–C) and scanning electron micrographs (D–H) of carinal canals (A, B, D), vallecular canals (C, E), central cavities (F) and xylem (G, H) of *E. ramosissimum*. (A) Transverse section of the carinal canal and associated parenchyma showing the electron-dense lining of the carinal canal. (B) Detail of electron-dense lining. (C) Transverse section showing the lining of the vallecular canal. (D) Smooth inner surface of the carinal canal. (E, F) Rough inner surface of the vallecular canal (E) and central cavity (F). (G) Multiseriate pitting of nodal xylem elements. (H) Scalariform pitting of internodal metaxylem elements. Scale bars: (A, D–H) = 10 μm; (B, C) = 2 μm.

fused into a sheath surrounding the base of the next higher internode, are the continuation of the ridges of the lower internode.

DISCUSSION

Our study revealed some specific spatial distributions of cell wall epitopes in the stem of *E. ramosissimum*, and provided new data on its general anatomy.

A range of monoclonal antibodies was used to map the distribution of specific cell wall epitopes in *E. ramosissimum* stems, with a focus on the carinal canals. Although positive results with labelled antibodies demonstrate the presence of epitopes, negative results do not necessarily imply their absence, as epitopes can be masked by various polysaccharides within cell wall materials even when all cell wall layers are exposed during sectioning (Marcus *et al.*, 2008, 2010). The anti-extensin antibodies LM1 and JIM20 bound strongly to the lining of carinal canals, and additional, but very weak, binding to cell wall corners of cortical parenchyma was observed after pectate lyase treatment. To date, extensins have been proposed to be structural cell wall proteins that may play a significant role during growth and development, wound healing and plant defence reactions (Albersheim *et al.*, 2010). They can be insolubilized in the cell wall through covalent and/or non-covalent cross-linking with themselves and/or other cell wall polymers (Johnson *et al.*, 2003). The presence of JIM5, LM18 and LM19 epitopes and the absence of JIM7 and LM20 epitopes indicated the occurrence of largely de-esterified homogalacturonan in the linings of the carinal canals (Willats *et al.*, 2001). The co-localization of extensins and highly de-esterified pectins in these linings may suggest some cross-linking between these polymers. Similar co-localization has been reported in cotton fibres (Vaughn and Turley, 1999), in trichomes of mericarps of *Galium aparine* (Bowling *et al.*, 2008), in walls of cellulose-deficient, dichlobenil (DCB)-habituated BY-2 cells (Sabba *et al.*, 1999) and in intercellular pectic protuberances of *Asplenium aethiopicum* (Leroux *et al.*, 2007*b*). Covalent cross-linking between extensins and pectins has been reported by Qi and Mort (1995). Alternatively, extensins could interfere ionically with the calcium cross-linking of pectic chains, forming weaker gels, which suggests a role for extensins in modulating the pectin gel network (MacDougall *et al.*, 2001). Extensins can be cross-linked within just a few minutes of wounding, mediated by the release of hydrogen peroxide and catalysed by a wall peroxidase (Cooper and Varner, 1984). Potential cross-linking in the lining of the carinal canals was assessed through a peroxidase activity test, and, though we supplied the sample with exogenous H_2O_2, we only observed weak staining of the lining of the carinal canals. Hence we did not obtain strong evidence suggesting peroxidase-mediated cross-linking of extensins. Furthermore, the structural and/or regulatory role of extensins as well as their potential interaction with other polymers in the lining of carinal canals remain unclear and need to be studied in further detail. We also detected xyloglucan epitopes (LM15/CCRC-M1) in the lining of carinal canals. In this case the epitopes were detected in the lining of carinal canals only after pectate lyase treatment, indicating an intimate association with the pectic homogalacturonan of the lining material. This is distinct from xyloglucan epitope detection in the phloem sieve cells and indicates a distinct disposition of xyloglucan in relation to other cell wall components and unique cell wall architecture in the carinal canal lining. Although it was shown that a molecularly distinct matrix containing de-esterified homogalacturanon, xyloglucan, extensin and cellulose lines the carinal canals, detailed immunogold localization studies are required to assess the spatial distribution of each of these cell wall components fully. In *E. arvense*, LM11, recognizing unsubstituted xylan and arabinoxylan, bound to the lining of carinal canals (Sørensen *et al.*, 2008). However, a similar LM11 epitope distribution pattern was not observed in *E. ramosissimum* even following pectate lyase treatment. The binding pattern of the anti-MLG antibody (Biosupplies 400-3) in *E. ramosissimum* was different when compared with that observed by Sørensen *et al.* (2008) in *E. arvense*. Whereas labelling in *E. ramosissimum* was restricted to the strengthening tissue and some cortical cell walls, it was found to bind strongly to the epidermal and

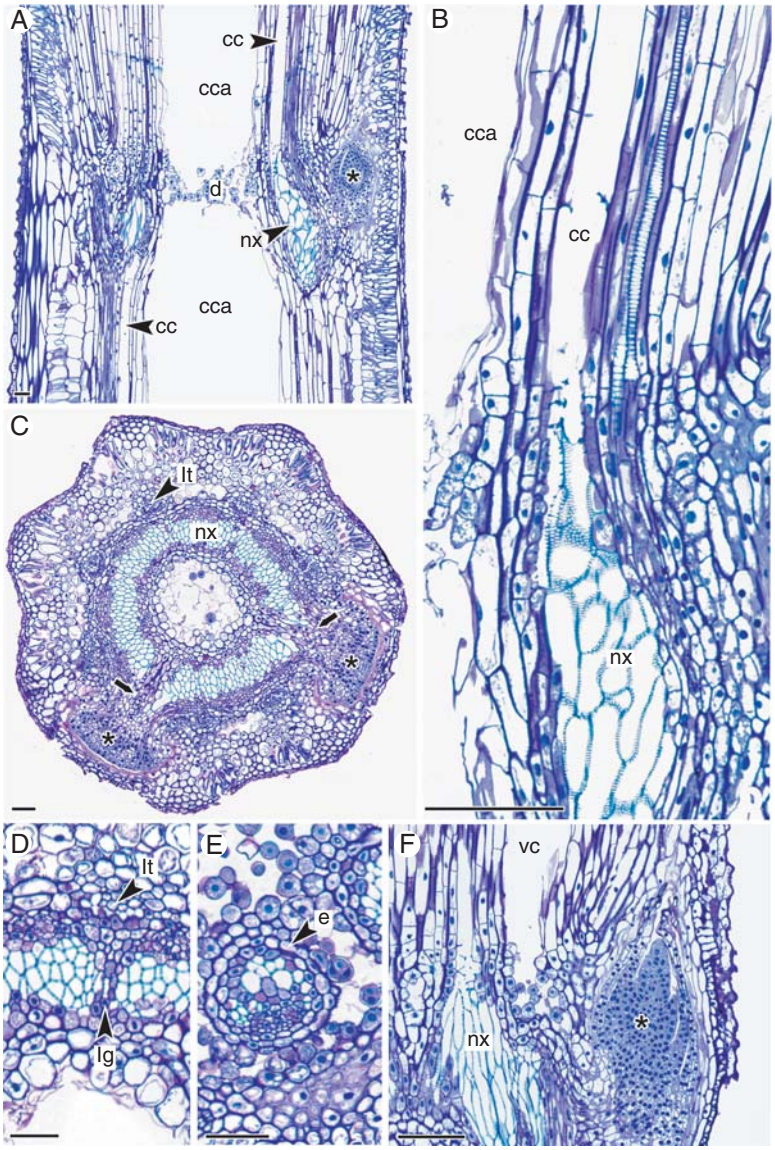

FIG. 5. Longitudinal (A, B, F) and transverse (C–E) sections of mature nodes of *E. ramosissimum*. (A) Nodal diaphragm (d) interrupting central cavities (cca) of consecutive internodes, and carinal canals (cc) connected to nodal xylem (nx). (B) Detail showing the connection of the carinal canal (cc) to nodal xylem (nx). (C) Node showing a temporary ectophloic sipholostele interrupted by two branch gaps (arrows), with leaf traces (lt) situated outside the stele. (D) Leaf trace (lt) with associated leaf gap (lg) at the base of the internode–node transition. (E) Later stage in node–internode transition with a dictyostele consisting of separated meristeles enclosed by an individual endodermis (e). (F) Nodal region showing the bottom of the vallecular canal (vc) separated by parenchyma from nodal xylem (nx). Asterisks indicate branch meristems. Scale bars = 100 μm.

cortical parenchyma cell walls in *E. arvense*. Furthermore, Sørensen *et al.* (2008) showed that the MLG epitopes were distributed throughout the cell walls of the strengthening tissue, while we only detected them in the inner region of these walls. Epitope masking and/or the developmental regulation of MLG incorporation in cell walls may account for the observed differences in epitope distribution.

Electron microscopy showed that the canals are lined with an electron-dense layer, which was absent in the vallecular canals and the central cavity. This electron-dense lining corresponds to the region labelled by the extensin, xyloglucan, cellulose and homogalacturonan antibodies, suggesting the presence of an additional cell wall matrix lining the canals. During light microscopic observations we also noticed that this lining was often thickened in older internodes. A similar moderate thickening was also reported by Bierhorst (1958*b*) for *E. sylvaticum*. Altogether these observations indicate that this lining is still being modified long after the carinal canals are formed and that additional cell wall material may be deposited in this lining by the cells surrounding these canals. Furthermore, the specialized cell wall matrix lining the carinal canals could be responsible for the smoothness of the carinal canals as observed by scanning electron microscopy.

Since the early detailed investigations on the anatomy of *Equisetum*, it is known that the nodes in *Equisetum* stems are produced in close succession at the shoot apex and that they become separated by the development of the internodes as a result of intercalary meristematic growth and subsequent

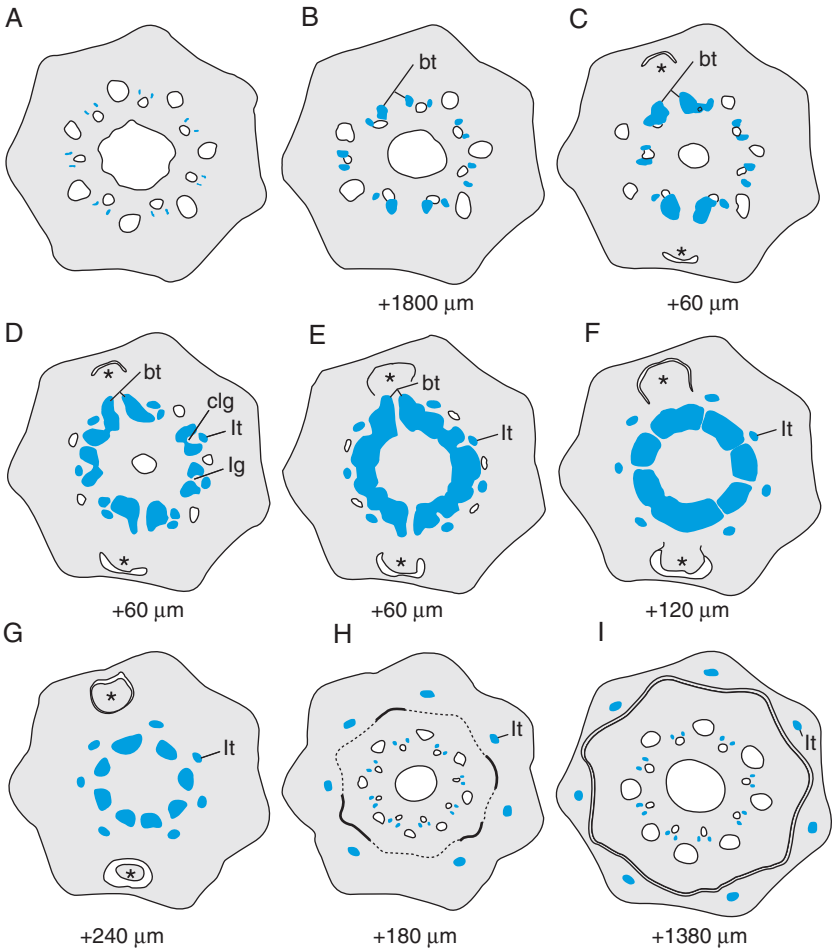

FIG. 6. Schematic drawings based on X-ray CT slices showing the distribution of xylem (blue zones) and carinal canals (blue contours) along the internode–node–internode transition. The distance from the preceding slice is indicated. (A) Typical internodal arrangement of vascular bundles with carinal canals and lateral xylem. (B, C) Extra tracheids extend the xylem between the lateral metaxylem and carinal canal, with outward extension initiating branch traces (bt). (D) Carinal canals replaced by xylem, with leaf traces (lt) branched off and leaving gaps (lg) or becoming closed at this early stage (clg). (E) Temporary ectophloic siphonostele interrupted by two branch traces (bt). (F, G) Fragmentation of nodal xylem into meristeles. (H, I) Separation of the leaf sheath and reappearance of the typical internodal arrangement of vascular bundles. Branch meristems are indicated with asterisks.

elongation (Browne, 1912, 1922; Barrat, 1920). The annular protoxylem elements interconnecting consecutive nodal xylem rings near the shoot apex are stretched and disrupted during the early stages of elongation of the internodes, leading to the formation of the carinal canals (Browne, 1912). The interconnection of carinal canals via the nodal xylem was first reported in *Equisetum* by Sykes (1906), confirmed to occur in *E. sylvaticum* by Bierhorst (1958*a*) and now also shown to be present in *E. ramosissimum*. Lateral xylem elements only differentiate after the formation of the central, as well as the carinal and vallecular canals, when the internode is fully stretched. The changes occurring during internode–node–internode transition in *E. ramosissimum* are similar to those described for *E. giganteum* (Browne, 1922) and *E. arvense* (Meyer, 1920). Several authors, e.g. Jeffrey (1899), Eames (1909, 1936), Meyer (1920), Smith (1955), Stewart (1983) and Kramer *et al.* (1995), stated or accepted that leaf traces in *Equisetum* are not associated with leaf gaps, and therefore considered these to represent microphylls. However, the presence of branching and telome-like leaves in fossil *Hyenia* and *Calamophyton*, the branching open venation pattern in extinct *Sphenophyllum* and *Archaeocalamites* (Lesquereux, 1879; Stewart, 1983; Kaplan, 2001), as well as the presence of leaf gaps in *E. giganteum* (Browne, 1922) and in *E. ramosissimum* (this study) suggest that leaves in horsetails are megaphyllous, which would confirm their separation from the Lycopsida and their closer alliance to true ferns (Pryer *et al.*, 2001).

The intimate connection of the smooth carinal canals to the nodal xylem indicates that these may represent specialized conducting canals. This was first suggested by Westermaier (1884), and later confirmed by Strasburger (1891), Sykes (1906), Meyer (1920), Buchholz (1921) and Bierhorst (1958*b*). They studied the water flow in stems of *Equisetum* using dye uptake experiments. Similar experiments have also been undertaken to show water flow in a wide range of monocots (Buchholz, 1921; Dong *et al.*, 1997). Using nuclear magnetic resonance microscopy, Xia *et al.* (1993) demonstrated water flow in the carinal canals of *E. arvense* (misidentified as *E. hyemale*). Their study revealed a relatively low velocity

of approx. 40 μm s^{-1}. This low flow rate most probably resulted from the nodal interruption consisting of very short xylem elements.

CONCLUSIONS AND FUTURE PERSPECTIVES

The connection of carinal canals from consecutive internodes by nodal xylem rings suggests that carinal canals function as water-conducting channels. At least during the elongation of the internodes, when the protoxylem has been disrupted and the metaxylem is not yet functional, the carinal canals are the only structures to transport water. Our immunocytochemical study revealed an extensin-rich cellulose–pectic homogalacturonan–xyloglucan cell wall matrix lining the carinal canals, which most probably corresponds to the electron-dense lining observed with transmission electron microscopy. How this distinct lining relates to the proposed water-conducting function requires further studies.

The distribution of some cell wall epitopes in stems of *E. ramosissimum* was different from that observed in *E. arvense* by Sørensen *et al.* (2008). This may show that the cell wall composition might be highly variable among related species. On the other hand, some of this variation might be caused by the fact that cell walls are highly dynamic and, hence, constantly remodelled during growth and development, and in response to environmental stress (Lee *et al.*, 2011). Therefore, an increased understanding of structural–functional relationships of polymers (and their interactions) is to be expected when their temporal and spatial occurrence is investigated at the cell type level in a taxonomically broad range of plants.

It would also be of interest to investigate the molecular composition of the linings of carinal canals of other *Equisetum* species, or of protoxylem lacunae in other plant taxa such as the intrafascicular canals in the quillwort *Isoetes* (Romeo *et al.*, 2000) and the protoxylem lacunae in the petioles and/or stems of many monocots such as *Nuphar* (Esau, 1965). Comprehensive imaging of cell wall architecture of water-conducting elements in a variety of plant taxa, including bryophytes, lycophytes, ferns and seed plants, has great potential to (*a*) provide insights into the evolution of vascular tissues and (*b*) to allow understanding of how cell wall composition and structure underpin the specialized function of water-transporting elements. For instance, the diversity observed in cell wall composition of water-conducting cells in bryophytes provides new evidence for the multiple origins of water-conducting cells (Ligrone *et al.*, 2002).

A large-scale survey of cell wall structure and composition across the plant kingdom may yield valuable new data which could contribute to our knowledge of cell wall evolution and diversity, as well as to our understanding of how cell wall architecture correlates with specialized properties of specific tissues or tissue types.

SUPPLEMENTARY DATA

Supplementary data are available at www.aob.oxfordjournals.org and consist of the following files. Figure S1: morphology of a stem of *E. ramosissimum* and X-ray CT images of internodes. Video: based on X-ray CT slices, showing the anatomically complex internode–node–internode transition (the video is approx. 145 Mb in size and in .avi format).

ACKNOWLEDGEMENTS

This study was supported by grant 1.5.157.10.N.00 from the Fund for Scientific Research-Flanders, Belgium (F.W.O-Vlaanderen) and the Systematics Research Fund (The Linnean Society of London). We thank Z. Popper for her thoughtful comments on an early version of the manuscript, and two anonymous reviewers for their useful comments and suggestions.

LITERATURE CITED

Albersheim P, Darvill A, Roberts K, Sederoff R, Staehelin A. 2010. *Plant cell walls: from chemistry to biology*. New York: Garland Science.

Barrat K. 1920. A contribution to our knowledge of the vascular system of the genus *Equisetum*. *Annals of Botany* **34**: 201–235.

Bateman RM. 1991. Palaeobiological and phylogenetic implications of anatomically preserved Archaeocalamites from the Dinantian of Oxford Bay and Loch Humpherey Burn, southern Scotland. *Palaeontographica* **223**: 1–59.

Bierhorst DW. 1958*a*. Vessels in *Equisetum*. *American Journal of Botany* **45**: 534–537.

Bierhorst DW. 1958*b*. The tracheary elements of *Equisetum* with observation on the ontogeny of the internodal xylem. *Bulletin of the Torrey Botanical Club* **85**: 416–433.

Bischoff GW. 1828. Die Chareen und Equiseteen. In: Bischoff GW. ed. *Die kryptogamischen Gewächse*. Nürnberg: J.L. Schrag, 1–60.

Bischoff GW. 1834. *Lehrbuch der Botanik. Erster Band. Allgemeine Botanik. I*. Stuttgart: E. Schweizerbart's Verlagshandlung.

Blake AW, McCartney L, Flint JE, *et al*. 2006. Understanding the biological rationale for the diversity of cellulose-directed carbohydrate-binding modules in prokaryotic enzymes. *Journal of Biological Chemistry* **281**: 29321–29329.

Bowling AJ, Maxwell BH, Vaughn KC. 2008. Unusual trichome structure and composition in mericarps of bedstraw (*Galium aparine* L.). *Protoplasma* **233**: 223–230.

Brongniart A. 1828. *Histoire des végétaux fossiles, ou recherches botaniques et géologiques sur les végétaux renfermés dans les diverses couches du globe. Tome premier*. Paris: G. Dufour & Ed. d'Ocagne.

Browne IMP. 1912. Contributions to our knowledge of the anatomy of the cone and fertile stem of *Equisetum*. *Annals of Botany* **26**: 663–703

Browne IMP. 1922. Anatomy of *Equisetum giganteum*. *Botanical Gazette* **73**: 447–468.

Buchholz M. 1921. Über die Wasserleitungsbahnen in den interkalaren Wachstumszonen monokotyler Sprosse. *Flora* **114**: 119–186.

Clausen MH, Willats WGT, Knox JP. 2003. Synthetic methyl hexagalacturonate hapten inhibitors of anti-homogalacturonan monoclonal antibodies LM7, JIM5 and JIM7. *Carbohydrate Research* **338**: 1797–1800.

Cooper JB, Varner JE. 1984. Cross-linking of soluble extensin in isolated cell walls. *Plant Physiology* **76**: 414–417.

Cormack BG. 1893. On a cambial development in *Equisetum*. *Annals of Botany* **7**: 62–82.

Currie HA, Perry CC. 2009. Chemical evidence for intrinsic 'Si' within *Equisetum* cell walls. *Phytochemistry* **70**: 5089–2095.

Des Marais DL, Smith AR, Britton DM, Pryer KM. 2003. Phylogenetic relationships and evolution of extant horsetails, *Equisetum*, based on chloroplast DNA sequence data (*rbcL* and *trnL-F*). *International Journal of Plant Sciences* **164**: 737–751.

Dong Z, McCully ME, Canny MJ. 1997. Does *Acetobacter diazothrophicus* live and move in the xylem of sugar cane stems? Anatomical and physiological data. *Annals of Botany* **80**: 147–158.

Eames AJ. 1909. On the occurrence of centripetal xylem in *Equisetum*. *Annals of Botany* **23**: 587–601.

Eames AJ. 1936. *Morphology of vascular plants. Lower groups (Psilophytales to Filicales)*. New York: McGraw-Hill.

Emberger L. 1944. *Les plantes fossiles dans leurs rapports avec les végétaux vivants (éléments de paléobotanique et de morphologie comparée).* Paris: Masson et Cie.

Esau K. 1965. *Plant anatomy.* New York: John Wiley.

Frank AB. 1877. Dritte Abtheilung. II. Cryptogamae L. In: Leunis J. ed. *Synopsis der Pflanzenkunde*. Hannover: Hahn'sche Buchhandlung, 1231–1961.

Fry SC, Nesselrode BH, Miller JG, Mewburn BR. 2008. Mixed-linkage (1→3, 1→4)-beta-D-glucan is a major hemicellulose of *Equisetum* (horsetail) cell walls. *New Phytologist* **179**: 104–115.

Gierlinger N, Sapei L, Paris O. 2008. Insights into the chemical composition of *Equisetum hyemale* by high resolution Raman imaging. *Planta* **227**: 969–980.

Guillon J-M. 2004. Phylogeny of horsetails (*Equisetum*) based on the chloroplast *rps4* gene and adjacent non coding sequences. *Systematic Botany* **29**: 251–259.

Guillon J-M. 2007. Molecular phylogeny of horsetails (*Equisetum*) including atpB sequences. *Journal of Plant Research* **120**: 569–574.

Gwynne-Vaughan DT. 1901. Remarks upon the nature of the stele in *Equisetum*. *Annals of Botany* **15**: 71–98.

Hauke RL. 1963. A taxonomic monograph of the genus *Equisetum* subgenus *Hippochaete*. *Beihefte Nova Hedwigia* **8**: 1–123.

Hauke RL. 1978. A taxonomic monograph of the genus *Equisetum* subgenus *Equisetum*. *Nova Hedwigia* **30**: 385–455.

Hauke RL. 1990. Equisetaceae. In: Kramer KU, Green PS. eds. *The families and genera of vascular plants, vol. I. Pteridophytes and gymnosperms*. Berlin: Springer-Verlag, 46–48.

Hirmer M. 1938. Articulatae. In: Verdoorn Fr. ed. *Manual of pteridology.* The Hague: Martinus Nijhoff, 511–521.

Jeffrey EC. 1899. The development, structure, and affinities of the genus *Equisetum*. *Memoirs of the Boston Society of Natural History* **5**: 155–190

Johnson KL, Jones BJ, Schulz CJ, Bacic A. 2003. Non-enzymic cell wall (glyco)proteins. In: Rose JKC. ed. *The plant cell wall*. Oxford: Blackwell Publishing, 111–154.

Jones L, Seymour GB, Knox JP. 1997. Localization of pectic galactan in tomato cell walls using a monoclonal antibody specific to (1→4)-β-D-galactan. *Plant Physiology* **113**: 1405–1412.

Kaplan DR. 2001. The science of plant morphology: definition, history, and role in modern biology. *American Journal of Botany* **88**: 1711–1741.

Karol KG, Arumuganathan K, Boore JL, *et al.* 2010. Complete plastome sequences of *Equisetum arvense* and *Isoetes flaccida*: implications for phylogeny and plastid genome evolution of early land plant lineages. *BMC Evolutionary Biology* **10**: 321. doi:10.1186/1471-2148-10-321.

Kenrick P, Crane PR. 1997. The origin and early evolution of plants on land. *Nature* **389**: 33–39.

Knox JP. 2008. Mapping the walls of the kingdom: the view from the horsetails. *New Phytologist* **179**: 1–3.

Kramer KU, Schneller JJ, Wollenweber E. 1995. *Farne und Farnverwandte. Bau, Systematik, Biologie*. Stuttgart: G. Thieme Verlag.

Lee KJD, Marcus SE, Knox JP. 2011. Plant cell wall biology: perspectives from cell wall imaging. *Molecular Plant* **4**: 212–219.

Leroux O, Van der Kinderen G, Viane RLL. 2007*a*. A sandwich-embedding method for oriented sectioning. *Journal of Microscopy* **227**: 79–82.

Leroux O, Knox JP, Leroux F, *et al.* 2007*b*. Intercellular pectic protuberances in *Asplenium*: new data on their composition and origin. *Annals of Botany* **100**: 1165–1173.

Leroux O, Leroux F, Bellefroid F, *et al.* 2009. A new preparation method to study fresh plant structures with X-ray computed tomography. *Journal of Microscopy* **233**: 1–4.

Lesquereux L. 1879. *Second geological survey of Pennsylvania: Report of progress. Atlas to the Coal flora of Pennsylvania and of the Carboniferous formation throughout the United States*. Harrisburg: Board of Commissioners.

Ligrone R, Vaughn KC, Renzaglia KS, Knox JP, Duckett JG. 2002. Diversity in the distribution of polysaccharide and glycoprotein epitopes in the cell walls of bryophytes: new evidence for the multiple evolution of water-conducting cells. *New Phytologist* **156**: 491–508.

MacDougall AJ, Brett GM, Morris VJ, Rigby NM, Ridout MJ, Ring SG. 2001. The effect of peptide–pectin interactions on the gelation behaviour of a plant cell wall pectin. *Carbohydrate Research* **335**: 115–126.

Marcus SE, Verhertbruggen Y, Hervé C, *et al.* 2008. Pectic homogalacturonan masks abundant sets of xyloglucan epitopes in plant cell walls. *BMC Plant Biology* **8**: 60. doi:10.1186/1471-2229-8-60.

Marcus SE, Blake AW, Benians TAS, *et al.* 2010. Restricted access of proteins to mannan polysaccharides in intact plant cell walls. *The Plant Journal* **64**: 191–203.

Masschaele BC, Cnudde V, Dierick M, Jacobs P, Van Hoorebeke L, Vlassenbroeck J. 2007. UGCT: new x-ray radiography and tomography facility. *Nuclear Instruments and Methods in Physics Research, Section A* **580**: 266–269.

McCartney L, Marcus SE, Knox JP. 2005. Monoclonal antibodies to plant cell wall xylans and arabinoxylans. *Journal of Histochemistry and Cytochemistry* **53**: 543–546.

Meikle PJ, Bonig I, Hoogenraad NJ, Clarke AE, Stone BA. 1991. The location of (1→3)-β-glucans in the cell walls of pollen tubes of *Nicotiana alata* using a (1→3)-β-glucan-specific monoclonal antibody. *Planta* **185**: 1–8.

Meikle PJ, Hoogenraad NJ, Bonig I, Clarke AE, Stone BA. 1994. A (1→3,1→4)-β-glucan-specific monoclonal antibody and its use in the quantitation and immunocytochemical location of (1→3,1→4)-β-glucans. *The Plant Journal* **5**: 1–9.

Meyer FJ. 1920. Das Leitungssystem von *Equisetum arvense. Jahrbuch für Wissenschaftliche Botanik* **59**: 263–286.

Milde J. 1867. Monographia Equisetorum. *Novorum Actorum Academiae Caesareae Leopoldino-Carolinae Germanicae Naturae Curiosorum* **32**: 1–607.

Ogura Y. 1972. *Comparative anatomy of vegetative organs of the pteridophytes*. Berlin: Gebruder Borntraeger.

Popper ZA, Fry SC. 2004. Primary cell wall composition of pteridophytes and spermatophytes. *New Phytologist* **164**: 165–174.

Pryer KM, Schneider H, Smith AR, Cranfill R, Wolf PG, Sipes SD. 2001. Horsetails and ferns are a monophyletic group and the closest relatives to seed plants. *Nature* **409**: 618–622.

Puhlmann J, Bucheli E, Swain MJ, *et al.* 1994. Generation of monoclonal antibodies against plant cell wall polysaccharides. I. Characterization of a monoclonal antibody to a terminal α-(1,2)-linked fucosyl-containing epitope. *Plant Physiology.* **104**: 699–710.

Qi X, Behrens BX, West PR, Mort AJ. 1995. Solubilization and partial characterization of extensin fragments from cell walls of cotton suspension cultures. *Plant Physiology* **108**: 1691–1701.

Qiu YL, Li LB, Wang B, *et al.* 2007. A nonflowering land plant phylogeny inferred from nucleotide sequences of seven chloroplast, mitochondrial, and nuclear genes. *International Journal of Plant Sciences* **168**: 691–708.

Rothwell GW. 1996. Pteridophytic evolution: an often underappreciated phytological success story. *Review of Palaeobotany and Palynology* **90**: 209–222.

Romeo D, Troia A, Burgarella C, Bellini E. 2000. Casparian strips in the leaf intrastelar canals of *Isoetes duriei* Bory, a Mediterranean terrestrial species. *Annals of Botany* **86**: 1051–1054.

Sabba RP, Durso NA, Vaughn KC. 1999. Structural and immunocytochemical characterization of the walls of dichlobenilhabituated BY-2 tobacco cells. *International Journal of Plant Sciences* **160**: 275–290.

Sadebeck R. 1902. Equisetaceae (der Jetztwelt). In: Engler A, Prantl K. eds. *Die Natürlichen Pflanzenfamilien*. Leipzig: Engelman, 520–548.

Schaffner JH. 1908. The air cavities of *Equisetum* as water reservoirs. *Ohio Naturalist* **9**: 393–394.

Smallwood M, Beven A, Donovan N, *et al.* 1994. Localization of cell wall proteins in relation to the developmental anatomy of the carrot root apex. *The Plant Journal* **5**: 237–246.

Smallwood M, Martin H, Knox JP. 1995. An epitope of rice threonine- and hydroxyproline-rich glycoprotein is common to cell wall and hydrophobic plasma membrane glycoproteins. *Planta* **196**: 510–522.

Smith GM. 1955. *Cryptogamic botany. Vol. 2. Bryophytes and Pteridophytes*, 2nd edn. New York: McGraw-Hill.

Sørensen I, Pettolino FA, Wilson SM, *et al.* 2008. Mixed-linkage (1→3), (1→4)-β-D-glucan is not unique to the poales and is an abundant component of *Equisetum arvense* cell walls. *The Plant Journal* **54**: 510–521.

Spatz HC, Emmans A. 2004. The mechanical role of the endodermis in *Equisetum* plant stems. *American Journal of Botany* **91**: 1936–1938.

Spatz HC, Köhler L, Speck T. 1998. Biomechanics and functional anatomy of hollow stemmed sphenopsids: I. *Equisetum giganteum* (Equisetaceae). *American Journal of Botany* **85**: 305–314.

Speck T, Speck O, Emmans A, Spatz HC. 1998. Biomechanics and functional anatomy of hollow stemmed sphenopsids. III. *Equisetum hyemale*. *Botanica Acta* **111**: 366–376.

Stanich NA, Rothwell GW, Stockey RA. 2009. Phylogenetic diversification of *Equisetum* (Equisetales) as inferred from Lower Cretaceous species of Britisch Columbia, Canada. *American Journal of Botany* **96**: 1289–1299.

Stenzel KG. 1861. Untersuchungen über Bau und Wachstum der Farne. II. Über Verjüngungserscheinungen bei den Farnen. *Novorum Actorum Academia Caesareae Leopoldinae-Carolinae Germanicae Naturae Curiosorum* **28**: 1–56.

Stewart WN. 1983. *Paleobotany and the evolution of plants*. Cambridge: Cambridge University Press.

Strasburger E. 1891. *Histologische Beiträge. Heft III. Ueber den Bau und die Verrichtungen der Leitungsbahnen in den Pflanzen.* Jena: G. Fischer.

Sykes MG. 1906. Tracheids in the nodal region of *Equisetum maximum*. *New Phytologist* **5**: 129–132.

Tournefort JP. 1719. *Institutiones Rei Herbariae. Editio tertia. Tomus I.* Paris: Typographia Regia.

Vaughn KC, Turley RB. 1999. The primary walls of cotton fibers contain an ensheathing pectin layer. *Protoplasma* **209**: 226–237.

Verhertbruggen Y, Marcus SE, Haeger A, *et al*. 2009*a*. Developmental complexity of arabinan polysaccharides and their processing in plant cell walls. *The Plant Journal* **59**: 413–425.

Verhertbruggen Y, Marcus SE, Haeger A, Ordaz-Ortiz JJ, Knox JP. 2009*b*. An extended set of monoclonal antibodies to pectic homogalacturonan. *Carbohydrate Research* **344**: 1858–1862.

Westermaier M. 1884. Untersuchungen über die Bedeutung todter Röhren und lebender Zellen für die Wasserbewegung in der Pflanze. *Sitzungsberichte der Königlich Preussischen Akademie der Wissenschaften zu Berlin* **4**: 1105–1117.

Willats WGT, Marcus SE, Knox JP. 1998. Generation of a monoclonal antibody specific to (1→5)-α-L-arabinan. *Carbohydrate Research* **308**: 149–152.

Willats WGT, McCartney L, Mackie W, Knox JP. 2001. Pectin: cell biology and prospects for functional analysis. *Plant Molecular Biology* **47**: 9–27.

Xia Y, Sarafis V, Campbell EO, Callaghan PT. 1993. Non invasive imaging of water flow in plants by NMR microscopy. *Protoplasma* **173**: 170–176.